

# SCIENTIFIC REPORTS



OPEN

## Hot Spots of Carbon and Alkalinity Cycling in the Coastal Oceans

Nicholas A. O'Mara<sup>1,2</sup> & John P. Dunne<sup>3</sup>

Ocean calcium carbonate ( $\text{CaCO}_3$ ) production and preservation play a key role in the global carbon cycle. Coastal and continental shelf (neritic) environments account for more than half of global  $\text{CaCO}_3$  accumulation. Previous neritic  $\text{CaCO}_3$  budgets have been limited in both spatial resolution and ability to project responses to environmental change. Here, a 1° spatially explicit budget for neritic  $\text{CaCO}_3$  accumulation is developed. Globally gridded satellite and benthic community area data are used to estimate community  $\text{CaCO}_3$  production. Accumulation rates ( $\text{PgC yr}^{-1}$ ) of four neritic environments are calculated: coral reefs/banks (0.084), seagrass-dominated embayments (0.043), and carbonate rich (0.037) and poor (0.0002) shelves. This analysis refines previous neritic  $\text{CaCO}_3$  accumulation estimates ( $-0.16$ ) and shows almost all coastal carbonate accumulation occurs in the tropics, >50% of coral reef accumulation occurs in the Western Pacific Ocean, and 80% of coral reef, 63% of carbonate shelf, and 58% of bay accumulation occur within three global carbonate hot spots: the Western Pacific Ocean, Eastern Indian Ocean, and Caribbean Sea. These algorithms are amenable for incorporation into Earth System Models that represent open ocean pelagic  $\text{CaCO}_3$  production and deep-sea preservation and assess impacts and feedbacks of environmental change.

Since the industrial revolution, fossil fuel burning and land use change have resulted in significant amounts of carbon dioxide release and global warming<sup>1</sup>. Thus far, about one third of this emitted  $\text{CO}_2$  has been taken up by the ocean<sup>2,3</sup>. This fraction is expected to grow to 90% on millennial timescales<sup>4</sup>. The ocean buffering capacity, or the ability to resist a change in pH, is dependent upon the ocean's carbon chemistry<sup>5</sup>. Carbonate mineral formation by biological precipitation and preservation within ocean sediment thus represents an important long-term storage mechanism in the global carbon cycle<sup>6</sup>. This process is highly susceptible to rising  $\text{pCO}_2$  and temperatures, and falling ocean pH which increases the solubility of carbonate minerals, reduces biological capacity to produce calcium carbonate ( $\text{CaCO}_3$ )<sup>7–11</sup>, and decreases rates of preservation within sediment<sup>12</sup>. While biogeochemically this set of processes serves as a compensating negative feedback increasing the ocean's ability to buffer anthropogenic  $\text{CO}_2$ , it is also expected to have severe deleterious impacts on coastal ecosystems<sup>13</sup>.

Many previous modeling efforts seeking to represent global production and burial of  $\text{CaCO}_3$  have focused on pelagic open ocean production and burial within deep sea sediments, while coastal areas have been largely excluded from global calculations<sup>14–16</sup>. Despite representing less than 7% of the seafloor, coastal and continental shelf (neritic) environments of less than 200 m water depth account for more than half of all  $\text{CaCO}_3$  accumulation in ocean sediment globally<sup>17–19</sup>. It has been suggested that short-term imbalances in neritic carbonate accumulation have caused many of the observed atmospheric carbon dioxide swings in the Pleistocene<sup>20</sup>. Therefore, understanding neritic carbonate budgets is crucially important to understand possible ecological and biogeochemical impacts and feedbacks of global climate change and ocean acidification.

Current estimates of neritic production are based on assumptions about global coverage and production averages of four community types: coral reefs, banks and coastal embayments, carbonate-rich shelves, and carbonate-poor shelves<sup>17–19</sup>. Fluxes within these environments were estimated based on global geochemical constraints, expert opinions, extrapolation to large spatial and temporal averages, and assumptions of the distribution of the four community types. In addition to the question of robustness of these simple empirical estimates, the lack of explicit controlling mechanisms provides no predictive power for estimating changes to these fluxes under different future environmental conditions.

In the present study, we take advantage of new, spatially-resolved physical and biogeochemical datasets to address several of these limitations to estimating the global neritic  $\text{CaCO}_3$  budget. These new datasets include

<sup>1</sup>Department of Earth and Environmental Sciences, Lamont-Doherty Earth Observatory, Columbia University, Palisades, NY, USA. <sup>2</sup>Department of Earth, Environmental and Planetary Sciences, Brown University, Providence, RI, USA. <sup>3</sup>NOAA Geophysical Fluid Dynamics Laboratory, 201 Forrestal Rd, Princeton, NJ, USA. Correspondence and requests for materials should be addressed to N.A.O. (email: [omara@ldeo.columbia.edu](mailto:omara@ldeo.columbia.edu))

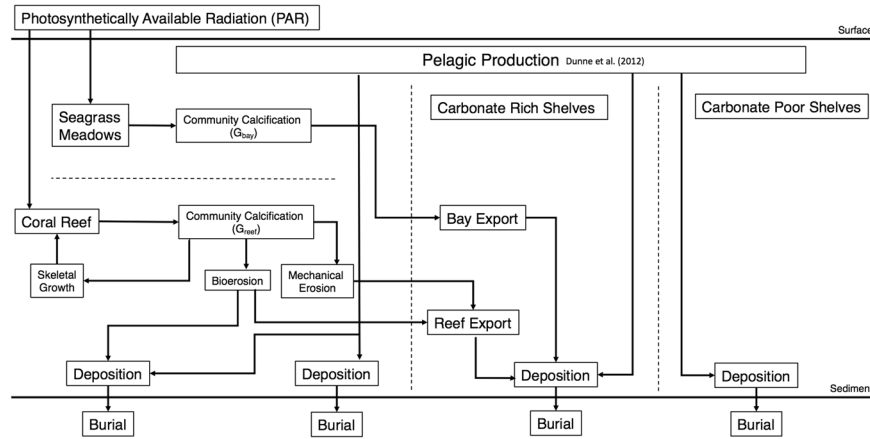


**Figure 1.** Conceptual model framework depicting the production, accumulation, and transfer of CaCO<sub>3</sub> within and between the four neritic regions: seagrass meadows, coral reefs, carbonate rich shelves and carbonate poor shelves.

high resolution bathymetric maps, satellite based estimates of pelagic CaCO<sub>3</sub> fluxes, global maps of CaCO<sub>3</sub> producing communities including corals and seagrass meadows, and new algorithms for terms in the CaCO<sub>3</sub> budget. These previously unavailable tools now make possible the spatially explicit characterization of the global neritic CaCO<sub>3</sub> environment.

### Methods

The neritic environment is represented here by a 1° × 1° spatial grid broken down into four community, or region, types: coral reefs, banks/embayments, carbonate-rich shelves, and carbonate-poor shelves for calculation of calcification, deposition and burial rates. In addition to these benthic fluxes, pelagic production estimates calculated by Dunne *et al.*<sup>16</sup> were extended over the neritic zone. A flow diagram of all of these budget calculations of each cell is provided in Fig. 1.

Globally gridded ocean datasets of annually averaged temperature<sup>21</sup>, salinity<sup>22</sup>, and nutrients<sup>23</sup> were taken from the World Ocean Atlas 2009. SeaWiFS photosynthetically available radiation (PAR)<sup>24</sup> and light extinction coefficients<sup>25</sup> were taken from the NASA Goddard Space Flight Center. Carbon chemistry and pH data were taken from the Carbon Dioxide Information Analysis Center (CDIAC) Global Ocean Data Analysis Project<sup>26</sup>. Surface and bottom water saturation states of calcite and aragonite were calculated according to the United Nations Educational, Scientific and Cultural Organization (1987) algorithm. High resolution bathymetric data were taken from the NOAA Etopo1 Global Relief Model<sup>27</sup>.

Coral reef areas were taken from the United Nations Environmental Programme World Conservation Monitoring Center (UNEP WCMC) GIS map of global coral area which represents global coral reef locations to a resolution of 500 m<sup>28</sup>. Coral area contained within each grid cell was then determined using ArcGIS software (<http://desktop.arcgis.com/en/arcmap/>) and assuming a constant scaling factor of 30% representing the percentage of live coral cover<sup>29</sup>. Coral CaCO<sub>3</sub> production by these corals was estimated as a function of sea surface temperature (SST), the saturation state of aragonite (Omega Aragonite), and light availability in the wavelengths photosynthetically available respiration (PAR) scaled by depth in the water column using the mean of the following three algorithms:

Kleypas *et al.*<sup>30</sup>

$$E_z = PAR * e^{-(K490)(Z)} \tag{1}$$

$$G_{reef1} = G_{max} * \tanh\left(\frac{E_z}{E_k}\right) \tag{2}$$

Lough<sup>31</sup>

$$G_{reef2} = 0.327 * (SST) - 6.98 \tag{3}$$

Silverman *et al.*<sup>32</sup>

$$G_i = \frac{24}{1000} (-0.0177 * SST^2 + 1.4697 * SST + 14.893) * (\Omega - 1)^{(0.628 * SST + 0.0985)} \tag{4}$$

$$G_{reef3} = k'_r * Gi * e^{-\left(\frac{k'_p(SST-T_{opt})}{\Omega^2}\right)^2}$$

$$G_{reef} = \left(\frac{G_{reef1} + G_{reef2} + G_{reef3}}{3}\right) * 0.3 \quad (5)$$

$G_{reef(1-3)}$  is the net community calcification predicted by each model,  $G_{reef}$  is the final average net community calcification used here,  $G_{max}$  is the maximum calcification given unlimited light,  $E_k$  is the light (PAR) incident on the surface of the ocean,  $E_z$  is the light reaching the depth of the coral,  $z$  is reef depth in meters,  $k_{490}$  is the light extinction coefficient for light of wavelength 490 nm, SST is the sea surface temperature overlying the coral reef,  $Gi$  is the inorganic community calcification,  $\Omega$  is the saturation state of aragonite,  $k'_r$  ( $38 \text{ m}^2 \text{ m}^{-2}$ ) and  $k'_p$  ( $1 \text{ }^\circ\text{C}^{-1}$ ) are scaling coefficients, and  $T_{opt}$  is the optimal temperature for growth determined from monthly average values of June in the northern hemisphere and December in the southern hemisphere.

Bioerosion of dead coral materials has been shown to correlate with trophic conditions of the waters the reefs inhabit, low bioerosion when waters are oligotrophic and high bioerosion when water are eutrophic<sup>33-35</sup>.

$$Bioerosion = 10,000 e^{-6e^{-5[PO_4^{3-}]}} \quad (6)$$

Values were thus determined using the above sigmoidal function Eq. (6) where bioerosion is dependent on the concentration of the phosphate ion ( $PO_4^{3-}$ ) in seawater. Half of this bioeroded material was assumed to remain on the reef while the other half is transported off the reef<sup>35</sup>.

Mechanical erosion is more uncertain than bioerosion and likely varies from reef to reef due to varying amounts of wave action and storm activity in different regions. Here a scalar 10% of  $G_{reef}$  was assumed to be removed from the reef due to mechanical erosion<sup>17</sup>. Total export from the reef is the sum of the mechanical erosion and the bioerosion losses.

Total deposition in the coral reef sediment is the sum of the remaining  $CaCO_3$  from bioerosion and the pelagic flux. Lacking a separate algorithm for the burial efficiency of aragonite, we assumed that aragonite burial efficiency behaved similar to calcite except for modulation via aragonite saturation state. The burial of aragonite from coral bioerosion and calcite from the pelagic flux within the sediment were thus both determined using the Dunne *et al.*<sup>16</sup> burial algorithm below:

$$\%Burial = \frac{F_{btm} - \Phi_R * F_{org}}{(\gamma * (1 - \Omega + \Phi_{org} * F_{org}))^\alpha * (F_{lith} + F_{btm})^\beta * C_0 + F_{btm}} \quad (7)$$

$F_{btm}$  is the calcite (aragonite) flux,  $F_{org}$  is the organic matter flux,  $F_{lith}$  is the terrigenous sediment flux,  $\Omega$  is the saturation state of calcite (aragonite),  $C_0$  is the density of calcite (aragonite),  $\gamma$  is the dissolution rate constant,  $\Phi_R$  and  $\Phi_{org}$  are dimensionless efficiency terms that affect dissolution at the sediment water interface and the pore water saturation state respectively.

Total accumulation within the coral reef environment is the sum of the burial of pelagic calcite, burial of bioerosion-created aragonite, and skeletal growth of corals.

Coastal embayments were represented here by areas where seagrass meadows were present from the United Nations Environmental Programme World Conservation Monitoring Center (UNEP WCMC) GIS map of global seagrass areas at a resolution of 500 m<sup>36</sup>. Seagrass, or bay area contained within each grid cell was then determined using ArcGIS software (<http://desktop.arcgis.com/en/arcmap/>).

Seagrass productivity was estimated as a function of SST and PAR in each grid cell where seagrasses were present<sup>37</sup>.

$$Productivity = \frac{0.584 * PAR + 16.06 * SST + 285}{2} \quad (8)$$

Estimates of productivity were then used to calculate the total biomass of seagrass present within each grid cell<sup>37</sup>.

$$Biomass = \frac{productivity - 318.846}{1.712} \quad (9)$$

Net community calcification in bay ecosystems ( $G_{bay}$ ; the sum of epiphyte organisms living on seagrass blades and mollusks living with the seagrass meadows in areas shallower than 30 m) was determined using the following equation<sup>38</sup>:

$$G_{bay} = 17.384 * Biomass + 670.26 \quad (10)$$

Mechanical erosion was again assumed to remove 10% of community production, like in reef systems, and biological erosion was assumed to export half of the remaining community production out of the seagrass meadow, while the rest is ultimately deposited to the sediment<sup>17,18</sup>. Similar to within coral reef sediments, the Dunne *et al.*<sup>16</sup> algorithm Eq. (7) was used to calculate burial within the bay sediment. However, the equation was slightly modified to incorporate the additional flux of organic matter from the seagrass blades themselves based on the estimate of Newell and Koch<sup>39</sup> that organic matter flux in seagrass meadows is approximately 70% from pelagic input.

Neritic Region	Area (10 <sup>12</sup> m <sup>2</sup> )		Flux (g C m <sup>-2</sup> yr <sup>-1</sup> )		Accumulation (Pg C yr <sup>-1</sup> )		Uncertainty	
	Iglesias-Rodriguez <i>et al.</i> (2002)	This Study	Iglesias-Rodriguez <i>et al.</i> (2002)	This Study	Iglesias-Rodriguez <i>et al.</i> (2002)	This Study	Iglesias-Rodriguez <i>et al.</i> (2002)	This Study (1σ)
Coral Reefs	0.6	0.25	140	334	0.084	0.084	±50%	±46%
Carbonate Shelves	10	7.30	3.8	5.34	0.038	0.037	>100%	±39%
Bays	0.8	0.34	30	125	0.024	0.043	±100%	±46%
Carbonate Poor Shelves	15	16.49	0.8	0.012	0.012	0.0002	>100%	±178%
Pelagic	—	24.38	—	0.012	—	0.0013	±100%	±85%
Benthic	26.4	24.38	—	—	0.158	0.163	±100%	±31%
Total					0.158	0.164		

**Table 1.** CaCO<sub>3</sub> benthic and pelagic flux and accumulation estimates for neritic regions from model output (this study) and previous estimates (Iglesias-Rodriguez *et al.*<sup>19</sup>).

$$\%Burial Bay = \frac{F_{btm} - \Phi_R * (F_{org}/0.7)}{(\gamma_*(1 - \Omega + \Phi_{org} * (F_{org}/0.7)))^\alpha * (F_{lith} + F_{btm})^\beta * C_0 + F_{btm}} \quad (11)$$

Unlike in the case of corals where we assume long term accumulation (burial) in skeletons, for seagrass bays we assume accumulation is equal to the burial within sediments because blade lifespans shorter than one year limit long-term storage of CaCO<sub>3</sub> within the living organisms<sup>40</sup>.

Carbonate-rich shelves are defined as the non-seagrass and non-coral areas shallower than 200 m within grid cells that contain either seagrasses or corals. Deposition of CaCO<sub>3</sub> is equal to export from either or both of those two communities spread evenly over the area of the grid cell not occupied by those communities in addition to the pelagic flux. Burial within carbonate-rich shelves are then determined using Eq. (7). Carbonate-poor shelves are defined as grid cells that contain shelf areas (<200 m) that do not contain any coral reefs or seagrass bays and the only CaCO<sub>3</sub> input is the pelagic flux. Burial is then calculated using Eq. (7).

Uncertainty in these budget estimates was determined using a Monte Carlo approach where each variable was allowed to vary uniformly by up to 50%. The distribution for each variable in the analysis was randomly sampled and carbonate accumulation rates were recalculated (n = 10,000) to estimate uncertainty in the CaCO<sub>3</sub> accumulation rate in each neritic region. The standard deviation of the resulting distributions (±1σ error) are shown in Table 1. While the total carbonate accumulation from the pelagic flux (178%) and carbonate-poor shelves (85%) remain quite uncertain, the uncertainty in the coral reefs (46%), carbonate-rich shelves (39%), and the bays (46%) are all less than the 50% variability introduced here suggesting that these uncertainties are only a product of the uncertainty in the underlying data that constrain this analysis. The total benthic accumulation is especially resilient to changes in the model parameters (31%).

## Results

The outputs of the described model framework represented spatially in Fig. 2 as well as values of the previous neritic carbonate budget estimate Iglesias-Rodriguez *et al.*<sup>19</sup> are summarized in Table 1.

We find total accumulation within the neritic zone study (0.164 Pg C yr<sup>-1</sup>) similar to the Iglesias-Rodriguez *et al.*<sup>19</sup> estimate (0.158 Pg C yr<sup>-1</sup>). Additionally, the pelagic contribution to neritic CaCO<sub>3</sub> accumulation (0.0013 Pg C yr<sup>-1</sup>) is much smaller than the benthic contribution (0.163 Pg C yr<sup>-1</sup>). The calculated accumulation within coral reef communities is approximately 0.084 (Pg C yr<sup>-1</sup>) and is actually identical to the prediction of the Iglesias-Rodriguez *et al.*<sup>19</sup> estimate despite varying estimates of coral reef area and fluxes of CaCO<sub>3</sub>. Likewise, we find very similar values for carbonate-rich shelf accumulation and flux rates despite slightly different total region areas. However, we find much higher flux and accumulation rates in bay sediment despite a smaller region areas and much lower carbonate-poor shelf flux and accumulation rates despite a larger region area than do Iglesias-Rodriguez *et al.*<sup>19</sup>.

As expected from their physiology, over 99% of warm water coral reef calcification is meridionally restricted to the tropics, and over half (53%) is restricted to 1/6th of the planet in the Western Tropical Pacific, from 120°E to the date line. The area west of 120°E into the Eastern Indian ocean at 90°E accounts for another 16%, and the Caribbean another 11%. Less expected, the distribution of both carbonate rich shelves (96%) and bays (93%) are also found to be restricted into the tropics (30°N–30°S). Burial of these CaCO<sub>3</sub> regimes are more broadly distributed across the tropical coastal regions with only 37% shelf and 28% bay burial in the Western Pacific, and the Caribbean accounting for a full 20% of bay burial (Table 2).

By extending past spatially explicit analysis into neritic regions, this study completes the global, spatially explicit picture of neritic and pelagic CaCO<sub>3</sub>. Figure 3 shows these neritic CaCO<sub>3</sub> burial fluxes determined here plotted along with previous estimates for the pelagic ocean<sup>16</sup>. The relatively intense local burial of CaCO<sub>3</sub> in neritic regions and the regionally focused burial in the Western Tropical Pacific and Atlantic Oceans illustrate the potential for neritic burial to influence both the meridional and interbasin structure in CaCO<sub>3</sub> burial. While pelagic burial is dominated by the North Atlantic, neritic burial is dominated by the tropics with the Western Tropical Pacific accounting for half of the global total.

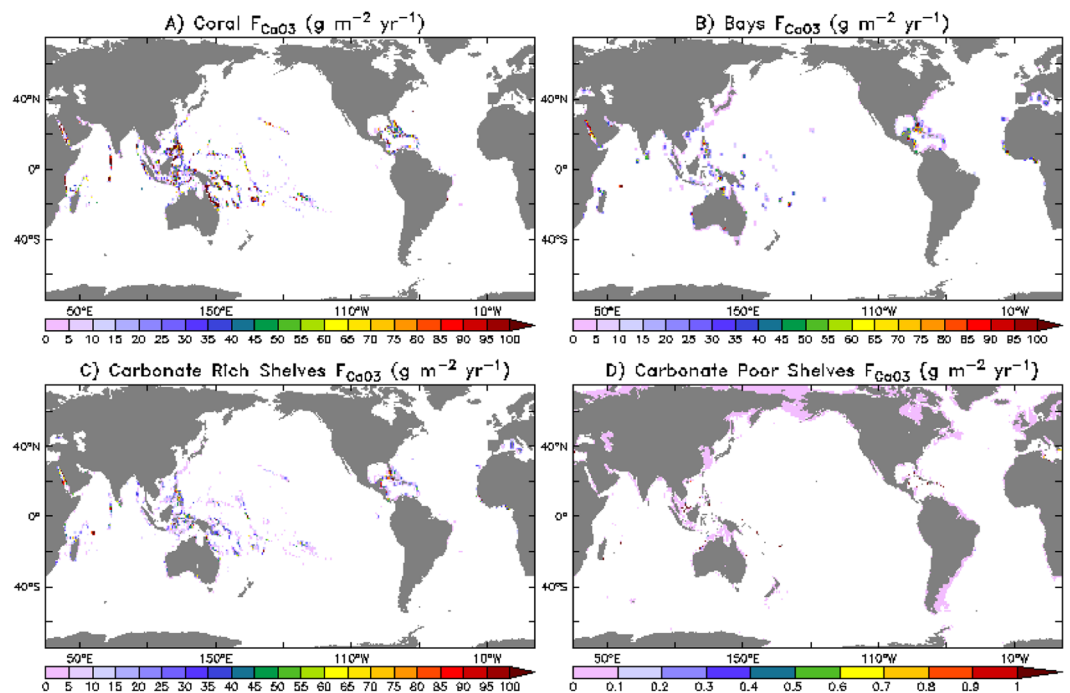


**Figure 2.** Global maps of model derived carbonate burial fluxes in (A) coral reefs, (B) seagrass bays, (C) carbonate rich shelves, and (D) carbonate poor shelves generated using the data analysis tool Ferret (v7) (<http://ferret.pmel.noaa.gov/Ferret>).

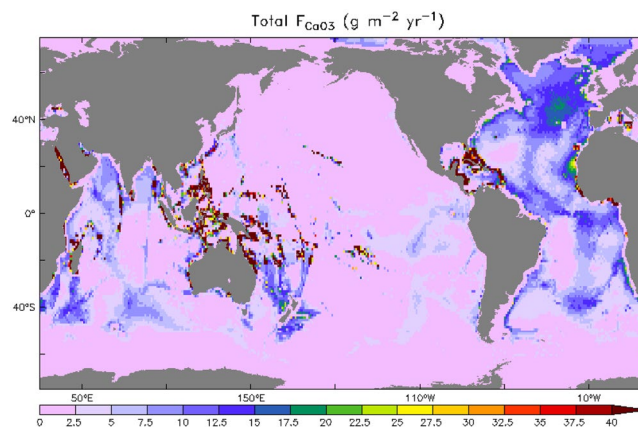


**Figure 3.** Global map of seafloor carbonate burial flux including both the neritic zone (this study) and the deep sea (Dunne *et al.*<sup>16</sup>) generated using the data analysis tool Ferret (v7) (<http://ferret.pmel.noaa.gov/Ferret>).

Neritic Region	Total Accumulation (Pg C yr <sup>-1</sup> )	Total Area (10 <sup>12</sup> m <sup>2</sup> )	Western Pacific (120°E–180°) %	Eastern Indian/Oceania (90°E–120°E) %	Caribbean (90°W–60°W, 8°N–31°N) %
Coral Reefs	0.084	0.25	53	16	11
Carbonate Shelves	0.037	7.30	37	9	17
Bay	0.043	0.34	28	10	20

**Table 2.** Regional % contribution of the Western Pacific Ocean, Eastern Indian Ocean/Oceania, and the Caribbean Sea to the total accumulation of CaCO<sub>3</sub> in coral reefs, carbonate shelves, and bays determined from

## Discussion

The Iglesias-Rodriguez *et al.*<sup>19</sup> CaCO<sub>3</sub> budget estimate of coral reef accumulation relied heavily upon assumptions made on the spatial extent, production, and burial rates within coral communities globally. Many of these assumptions are carried over from previous carbonate budget analyses<sup>17,18</sup>, which due to limited measurements

of locations of coral reefs assumed corals inhabited all environments suitable for growth, resulting in over estimations of total global coral areas  $0.6 \times 10^{12} \text{ m}^2$  compared to modern maps  $0.25 \times 10^{12} \text{ m}^2$ . Despite this over estimation of spatial extent, spurious Holocene accumulation averages, assumptions about large reductions of calcification in lagoon areas, and difficulty in measuring coral skeletal growth resulted in underestimations of total annual accumulation rates.

Carbonate-rich shelf environment estimates predicted by this model agree well with the Iglesias-Rodriguez *et al.*<sup>19</sup> estimates which provides increased confidence in the magnitude of these fluxes on the global scale. More importantly, this good comparison provides us with the additional opportunity to leverage the geographically explicit nature of our dataset and resolve region specific fluxes beyond a simple global budget and highlight 'hot spots' in the carbon cycle. The lower global area here is compensated by a higher average area-specific flux. In contrast, the model developed here predicts much higher accumulation rates of calcium carbonate within coastal embayment regions, or seagrass meadows, than previous estimates. Initial estimates of bank and bay areas were defined as regions shallower than 50 m and 30 m respectively that are partially surrounded by land, and assumed to be dominated by benthic algae rather than corals<sup>17</sup>. This resulted in a large over estimation of total bay area ( $0.8 \times 10^{12} \text{ m}^2$ ) in combination with limited sampling and reliance on long-term average deposition rates resulted in underestimates of deposition within these environments. This study takes a more specific approach in defining embayments as only those enclosed areas containing benthic seagrass communities.

A recent literature review<sup>41</sup> of global seagrass meadow  $\text{CaCO}_3$  burial, estimated that seagrass meadows have a range between  $0.177\text{--}0.6 \times 10^{12} \text{ m}^2$  and an accumulation rate of  $0.022\text{--}0.076 \text{ Pg C yr}^{-1}$  and a flux rate of  $126.3 \pm 0.7 \text{ gC m}^{-2} \text{ yr}^{-1}$ . The total area ( $0.34 \times 10^{12} \text{ m}^2$ ), accumulation rate ( $0.043 \text{ Pg C yr}^{-1}$ ), and flux values ( $125 \text{ gC m}^{-2} \text{ yr}^{-1}$ ) predicted by this model agree well with this study, which give credibility to the present estimates over previous attempts.

Carbonate-poor shelves have been predicted<sup>19</sup> to accumulate as much as  $0.012 \text{ Pg C yr}^{-1}$ . The present study predicts a vastly smaller annual accumulation of  $0.0002 \text{ Pg C yr}^{-1}$ . Production rates of carbonate are based on the dubious assumption that production in the sediment must exceed surface pelagic production<sup>18</sup>. This assumption allowed for carbonate-poor shelves to balance the biogeochemical gap between the measured fluvial ( $1.3 \text{ Tg C yr}^{-1}$ )<sup>42</sup> and estimated hydrothermal ( $0.3 \text{ Tg C yr}^{-1}$ )<sup>43</sup> and groundwater ( $0.5 \text{ Tg C yr}^{-1}$ )<sup>18</sup> inputs with total neritic accumulation, i.e. the estimates of coral reefs, bays, and carbonate-rich shelves<sup>18</sup>. This model, however, assumes benthic production of carbonate in carbonate-poor shelves equals pelagic input. The present study shows that larger predicted fluxes within coastal bay environments make this budget-based carbonate-poor shelf production assumption unnecessary as the flux is instead estimated explicitly.

Complementary to information about global  $\text{CaCO}_3$  production in various neritic zone environments, this analysis has further revealed three key coastal areas, or hot spots, in the Western Pacific Ocean, Eastern Indian Ocean, and Caribbean Sea that together represent more than half of the global coastal carbonate burial flux. The 'hot spots' the small coastal areas in these three geographic regions represent important focal points in the global coastal carbonate budget and thus warrant increased study and protective measures to mitigate large-scale anthropogenic perturbations to global carbonate budget.

The Iglesias-Rodriguez *et al.*<sup>19</sup> budget approximated uncertainties on the order of 50 to  $>100\%$ ; here we find similar errors ranging 31 to 178%. However, these new estimates have the added benefit of coming from a quantitatively defined model framework and thus represent a refinement of previous qualitative estimates. Furthermore, we demonstrate significant reductions in uncertainty estimates of carbonate rich shelves, bays, and total benthic accumulation. Unfortunately, our ability to ground-truth estimates for the  $\text{CaCO}_3$  budget determined here is limited by the paucity of relevant independent observational data. In contrast to the more spatially homogenous deep sea sediments, the heterogeneity of coastal carbonate producing ecosystems makes it difficult to extrapolate from single point measurements to global or even regional accumulation rates. Future sampling will allow for local comparisons between observed accumulation rates and predictions from this model. Despite the uncertainty of our results, this approach represents a carefully constructed null hypothesis for the role of carbonate producing ecosystems in the coastal ocean alkalinity budget.

There are several aspects of this study that warrant further investigation. Foremost among these would be to improve both the representation of heterogeneity at the local spatial scale within these environments and the mechanistic representation of these calcite and aragonite producing ecosystems to better capture their potential vulnerability to dissolution with enhanced ocean acidification. For example, live coral cover percentages, assumed here to be 30%, and mechanical erosion rates of reefs, assumed here to be 10% of net calcification, are in reality regionally variable. This study assumed simple, globally applicable production rates for coral, seagrass, and shellfish communities that are, in reality, likely highly variable. Furthermore, it does not account for the potential role of direct human actions such as pollution, habitat destruction, and fishing that are also known to have deleterious impacts<sup>44,45</sup>. Finally, while this model can project the potential response of the global neritic carbonate cycle, it cannot resolve the role of local heterogeneity in habitat and productivity in modulating sensitivity of carbonate producing ecosystems to environmental stressors. Such deficiencies in the current approach should be addressed with targeted and comprehensive process studies in these dynamic coastal environments.

## Conclusions

In this study, we address several deficiencies with previous estimates of neritic  $\text{CaCO}_3$  accumulation by (1) incorporating explicitly measured areas of neritic community types rather than hypothetical/potential areas, (2) spatially explicit rates of  $\text{CaCO}_3$  production and burial from an expanded observational database, (3) improved regional information and predictive power about future alterations to  $\text{CaCO}_3$  accumulation as a result of environmental change.

In its spatially explicit and comprehensive synthesis of the neritic  $\text{CaCO}_3$  budget, this study improves upon past estimates and creates a set of parameterizations that predict fluxes of  $\text{CaCO}_3$  within the neritic zone using

updated global maps of community areas and environmental constraints to estimate CaCO<sub>3</sub> accumulation rates. Model output (1) confirms prediction of dominance of benthic over pelagic production in the neritic zone, (2) corroborates current total neritic CaCO<sub>3</sub> accumulation with coral reefs contributing approximately half of the total and carbonate rich bays and shelves each contributing about a quarter, but predicts lower and higher rates in carbonate-poor shelves and embayments respectively, (3) despite only representing only 7% of the seafloor, neritic environments account for more than half of the total ocean annual CaCO<sub>3</sub> burial flux and almost entirely restricted to the tropical oceans with more than half of coral burial contained within the Western Tropical Pacific and total coastal burial contained within three hot spots, and (4) is readily amenable to implementation in global earth system models of carbon cycle impacts and feedbacks on ocean carbon uptake under environmental change. Future research is needed on the role of local heterogeneity in habitat, productivity, and human activity in modulating sensitivity of carbonate producing ecosystems to environmental stressors to improve regional and global scale predictions of how ocean acidification will influence carbonate-producing ecosystems.

## Data Availability

All datasets used for this analysis are available from their respective intext citations. The resulting carbonate flux data generated by this study can be found in the Supplementary Data for this article.

## References

- Solomon, S. *et al.* *Climate Change 2007: The Physical Science Basis: Contribution of Working Group I to the Fourth Assessment Report of the Intergovernmental Panel on Climate Change*. (New York: Cambridge Univ. Press 2007).
- Sabine, C. L. The Oceanic Sink for Anthropogenic CO<sub>2</sub>. *Science* **305**, 367–371 (2004).
- Sabine, C. L. & Feely, R. A. The oceanic sink for carbon dioxide. *Greenhouse gas sinks* **31** (2007).
- Houghton, J. T. *Climate change 2001 the scientific basis*. (Cambridge University Press, 2001).
- Eggleston, E. S., Sabine, C. L. & Morel, F. M. M. Revelle revisited: Buffer factors that quantify the response of ocean chemistry to changes in DIC and alkalinity. *Global Biogeochemical Cycles* **24** (2010).
- Metz, B. *Carbon dioxide capture and storage: IPCC special report*. (World Meteorological Organization, 2006).
- Caldeira, K. & Wickett, M. E. Oceanography: Anthropogenic carbon and ocean pH. *Nature* **425**, 365–365 (2003).
- Caldeira, K. Ocean model predictions of chemistry changes from carbon dioxide emissions to the atmosphere and ocean. *Journal of Geophysical Research* **110** (2005).
- Feely, R. A. Impact of Anthropogenic CO<sub>2</sub> on the CaCO<sub>3</sub> System in the Oceans. *Science* **305**, 362–366 (2004).
- Orr, J. C. *et al.* Anthropogenic ocean acidification over the twenty-first century and its impact on calcifying organisms. *Nature* **437**, 81–86 (2005).
- Fabry, V. J., Seibel, B. A., Feely, R. A. & Orr, J. C. Impacts of ocean acidification on marine fauna and ecosystem processes. *ICES Journal of Marine Science* **65**, 414–432 (2008).
- Hales, B. & Emerson, S. Calcite dissolution in sediments of the Ceara Rise: *In situ* measurements of porewater O<sub>2</sub>, pH, and CO<sub>2</sub>(aq). *Geochimica et Cosmochimica Acta* **61**, 501–514 (1997).
- Doney, S. C. *et al.* Ocean acidification: the other CO<sub>2</sub> problem (2009).
- Gehlen, M. *et al.* Reconciling surface ocean productivity, export fluxes and sediment composition in a global biogeochemical ocean model. *Biogeosciences* **3**, 521–537 (2006).
- Ridgwell, A. & Hargreaves, J. C. Regulation of atmospheric CO<sub>2</sub> by deep-sea sediments in an Earth system model. *Global Biogeochemical Cycles* **21** (2007).
- Dunne, J. P., Hales, B. & Toggweiler, J. R. Global calcite cycling constrained by sediment preservation controls. *Global Biogeochemical Cycles* **26** (2012).
- Milliman, J. D. Production and accumulation of calcium carbonate in the ocean: Budget of a nonsteady state. *Global Biogeochemical Cycles* **7**, 927–957 (1993).
- Milliman, J. D. & Droxler, A. W. Neritic and pelagic carbonate sedimentation in the marine environment: ignorance is not bliss. *Geologische Rundschau* **85**, 496–504 (1996).
- Iglesias-Rodriguez, M. D. *et al.* Progress made in study of oceans calcium carbonate budget. *Eos, Transactions American Geophysical Union* **83**, 365–375 (2002).
- Walker, J. C. G. & Opdyke, B. C. Influence of variable rates of neritic carbonate deposition on atmospheric carbon dioxide and pelagic sediments. *Paleoceanography* **10**, 415–427 (1995).
- Locarnini, R. A. *et al.* World Ocean Atlas 2009, Volume 1: Temperature. Levitus, S., Ed. NOAA Atlas NESDIS 68, U.S. Government Printing Office, Washington, D.C., 184 pp (2010).
- Antonov, J. I. *et al.* World Ocean Atlas 2009, Volume 2: Salinity. Levitus, S., Ed. NOAA Atlas NESDIS 69, U.S. Government Printing Office, Washington, D.C., 184 pp (2010).
- Garcia, H. E. *et al.* World Ocean Atlas 2009, Volume 4: Nutrients (phosphate, nitrate, silicate). Levitus, S., Ed. NOAA Atlas NESDIS 71, U.S. Government Printing Office, Washington, D.C., 398 pp (2010).
- Feldman, G. C. & McClain, C. R. Sea-viewing Wide Field-of-view Sensor (SeaWiFS) Photosynthetically Available Radiation Data; Reprocessing, NASA OB.DAAC, Greenbelt, MD, USA, <https://doi.org/10.5067/ORBVIEW-2/SEAWIFS/L3B/PAR/2014> (2014a).
- Feldman, G. C. & McClain, C. R. Sea-viewing Wide Field-of-view Sensor (SeaWiFS) Downwelling Diffuse Attenuation Coefficient Data; Reprocessing, NASA OB.DAAC, Greenbelt, MD, USA, <https://doi.org/10.5067/ORBVIEW-2/SEAWIFS/L3B/KD/2014> (2014b).
- Key, R. M. *et al.* A global ocean carbon climatology: Results from Global Data Analysis Project (GLODAP). *Global Biogeochemical Cycles* **18** (2004).
- Amante, C. & Eakins, B. W. ETOPO1 1 Arc-Minute Global Relief Model: Procedures, Data Sources and Analysis. NOAA Technical Memorandum NESDIS NGDC-24. *National Geophysical Data Center, NOAA*, <https://doi.org/10.7289/V5C8276M>. (2009).
- UNEP-WCMC, WorldFish Centre, WRI, TNC. Global distribution of warm-water coral reefs, compiled from multiple sources including the Millennium Coral Reef Mapping Project. Version 1.3. Includes contributions from IMaRS-USF and IRD (2005), IMaRS-USF (2005) and Spalding *et al.* (2001). Cambridge (UK): UNEP World Conservation Monitoring Centre, <http://data.unep-wcmc.org/datasets/1> (2010).
- Hodgson, G., Liebler, J. & Hassan, M. *The global coral reef crisis: trends and solutions*. (Reef Check Foundation, 2002).
- Kleypas, J. A. Modeled estimates of global reef habitat and carbonate production since the Last Glacial Maximum. *Paleoceanography* **12**, 533–545 (1997).
- Lough, J. Coral calcification from skeletal records revisited. *Marine Ecology Progress Series* **373**, 257–264 (2008).
- Silverman, J., Lazar, B. & Erez, J. Effect of aragonite saturation, temperature, and nutrients on the community calcification rate of a coral reef. *Journal of Geophysical Research* **112** (2007).

33. Hallock, P. The role of nutrient availability in bioerosion: Consequences to carbonate buildups. *Palaeogeography, Palaeoclimatology, Palaeoecology* **63**, 275–291 (1988).
34. Chazottes, V., Campion-Alsumard, T. & Peyrot-Clausade, M. Bioerosion rates on coral reefs: interactions between macroborers, microborers and grazers (Moorea, French Polynesia). *Palaeogeography, Palaeoclimatology, Palaeoecology* **113**, 189–198 (1995).
35. Glynn, P. W. & Manzello, D. P. Bioerosion and Coral Reef Growth: A Dynamic Balance. *Coral Reefs in the Anthropocene* 67–97 (2015).
36. UNEP-WCMC, Short FT. Global Distribution of Seagrasses (version 3). Third update to the data layer used in Green and Short (2003), superseding version 2. Cambridge (UK): UNEP World Conservation Monitoring Centre, <http://data.unep-wcmc.org/datasets/7> (2005).
37. Plus, M., Deslous-Paoli, J.-M., Auby, I. & Dagault, F. Factors influencing primary production of seagrass beds (*Zostera noltii* Hornem.) in the Thau lagoon (French Mediterranean coast). *Journal of Experimental Marine Biology and Ecology* **259**, 63–84 (2001).
38. Enríquez, S. & Schubert, N. Direct contribution of the seagrass *Thalassia testudinum* to lime mud production. *Nature Communications* **5** (2014).
39. Newell, R. I. E. & Koch, E. W. Modeling seagrass density and distribution in response to changes in turbidity stemming from bivalve filtration and seagrass sediment stabilization. *Estuaries* **27**, 793–806 (2004).
40. Hemminga, M., Marbà, N. & Stapel, J. Leaf nutrient resorption, leaf lifespan and the retention of nutrients in seagrass systems. *Aquatic Botany* **65**, 141–158 (1999).
41. Mazarrasa, I. *et al.* Seagrass meadows as a globally significant carbonate reservoir. *Biogeosciences* **12**, 4993–5003 (2015).
42. Meybeck, M. Concentrations des eaux fluviales en éléments majeurs et apports en solution aux océans. *Rev. Geol. Dyn. Geogr. Phys* **21**, 215–246 (1979).
43. Villiers, S. D., Shen, G. T. & Nelson, B. K. The -temperature relationship in coralline aragonite: Influence of variability in and skeletal growth parameters. *Geochimica et Cosmochimica Acta* **58**, 197–208 (1994).
44. Crain, C. M., Kroeker, K. & Halpern, B. S. Interactive and cumulative effects of multiple human stressors in marine systems. *Ecology Letters* **11**, 1304–1315 (2008).
45. Harborne, A. R., Rogers, A., Bozec, Y.-M. & Mumby, P. J. Multiple Stressors and the Functioning of Coral Reefs. *Annual Review of Marine Science* **9**, 445–468 (2017).

## Acknowledgements

We thank the NOAA Ernest F. Hollings Undergraduate Scholarship Program for supporting Mr. O'Mara's summer research project at GFDL and Charles Stock, Robbie Toggweiler and an anonymous reviewer for providing valuable critical feedback. We also wish to acknowledge use of the Ferret program for analysis and graphics in this paper. Ferret is a product of NOAA's Pacific Marine Environmental Laboratory. (Information is available at <http://ferret.pmel.noaa.gov/Ferret/>).

## Author Contributions

N.A.O. and J.P.D. both contributed on all aspects of the work.

## Additional Information

**Supplementary information** accompanies this paper at <https://doi.org/10.1038/s41598-019-41064-w>.

**Competing Interests:** The authors declare no competing interests.

**Publisher's note:** Springer Nature remains neutral with regard to jurisdictional claims in published maps and institutional affiliations.



**Open Access** This article is licensed under a Creative Commons Attribution 4.0 International License, which permits use, sharing, adaptation, distribution and reproduction in any medium or format, as long as you give appropriate credit to the original author(s) and the source, provide a link to the Creative Commons license, and indicate if changes were made. The images or other third party material in this article are included in the article's Creative Commons license, unless indicated otherwise in a credit line to the material. If material is not included in the article's Creative Commons license and your intended use is not permitted by statutory regulation or exceeds the permitted use, you will need to obtain permission directly from the copyright holder. To view a copy of this license, visit <http://creativecommons.org/licenses/by/4.0/>.

© The Author(s) 2019